Analysis of defect-related optical degradation of VCSILs for photonic integrated circuits

PROCEEDINGS OF SPIE

SPIEDigitalLibrary.org/conference-proceedings-of-spie

Analysis of defect-related optical degradation of VCSILs for photonic integrated circuits

M. Zenari, M. Buffolo, M. Fornasier, C. De Santi, J. Goyvaerts, et al.

M. Zenari, M. Buffolo, M. Fornasier, C. De Santi, J. Goyvaerts, A. Grabowski, J. Gustavsson, S. Kumari, A. Stassen, R. Baets, A. Larsson, G. Roelkens, G. Meneghesso, E. Zanoni, M. Meneghini, "Analysis of defect-related optical degradation of VCSILs for photonic integrated circuits," Proc. SPIE 12439, Vertical-Cavity Surface-Emitting Lasers XXVII, 124390E (15 March 2023); doi: 10.1117/12.2655696

SPIE.

Event: SPIE OPTO, 2023, San Francisco, California, United States

Analysis of defect-related optical degradation of VCSILs for photonic integrated circuits

M. Zenari[a*], M. Buffolo[a], M. Fornasier[a], C. De Santi[a], J. Goyvaerts[c], A. Grabowsky[d], J. Gustavsson[d], S. Kumari[c], A. Stassren[e], R. Baets[c], A. Larsson[d], G. Roelkens[c], G. Meneghesso[a], E. Zanoni[a] and M. Meneghini[a,b]

[a]Department of Information Engineering, University of Padova, via Gradenigo 6/B, 35131 Padova, Italy;
[b]Department of Physics and Astronomy, University of Padova, via Marzolo 8, 35131 Padova, Italy;
[c]Photonics Research Group, Ghent University-imec, Technologiepark-Zwijnaarde 126, 9052 Gent, Belgium;
[d]Department of Microtechnology and Nanoscience, Chalmers University of Technology, SE-412 96 Göteborg, Sweden;
[e]IMEC, Kapeldreef 75, 3001 Leuven, Belgium

ABSTRACT

Laser diodes are of paramount importance for on-chip telecommunications applications, and a wide range of sensing devices that require near-infrared sources. In this work, the devices under test are vertical-cavity silicon-integrated lasers (VCSILs) designed for operation at 845 nm in photonic integrated circuits (PICs). We focus on the analysis of the degradation of the optical performance during aging. To investigate the reliability of the devices, we carried out several stress tests at constant current, ranging from 3.5 mA to 4.5 mA representing a highly accelerated stress condition. We observed two different degradation modes. In the first part of the experiments, the samples exhibited a worsening of the threshold current, but the sub-threshold emission was unaffected by degradation. We associated this behavior to the diffusion of impurities that, from the p-contact, were crossing the upper mirror implying a worsening of the DBR optical absorption. In the second stage of the stress test, the devices showed a higher degradation rate of the threshold current, whose variation was found to be linearly correlated to the worsening of the sub-threshold emission. We related this second degradation mode to the migration of the same impurities degrading the top DBR that, when reaching the active region of the laser, induced an increase in the non-radiative recombination rate. In addition to that, we related the two degradation modes to the change in series resistance, which was ascribed to the resistivity increment of the top DBR first and of oxide aperture afterwards.

Keywords: Degradation, VCSIL, Diffusion, PICs

1. INTRODUCTION

In recent years, photonic integrated circuits (PICs) have been gaining momentum in the technology market. Indeed, the adoption of integrated photonics instead of electronics leads to different advantages such as higher speed of communication and lower energy consumption [1][2]. PICs have a variety of possible applications including telecommunications, integrated biosensors, and LIDAR systems [3][4]. All these applications require fast and energy-efficient light sources, that are, laser diodes. The most promising laser diodes for PICs are vertical-cavity surface-emitting lasers (VCSELs). These devices have been extensively adopted in data centers in the last thirty years, as they provide low threshold current (so low power consumption), high energy efficiency, and easy on-wafer testing [5]. Inside a photonic integrated circuit, the integration of III-V compound semiconductors onto silicon, SiN, or SOI (silicon on insulator) platforms is required as silicon is an indirect bandgap semiconductor which means that is unsuitable as an efficient light-emitter.

* michele.zenari@dei.unipd.it

Vertical-Cavity Surface-Emitting Lasers XXVII, edited by Chun Lei, Luke A. Graham,
Proc. of SPIE Vol. 12439, 124390E · © 2023 SPIE
0277-786X · doi: 10.1117/12.2655696

However, the direct growth of III-V materials onto these platforms is problematic as it causes the generation of defects arising from the material mismatch [6]. One promising solution is the utilization of the so-called micro-transfer printing technique [7]. This novel method consists in growing the lasers (in this case VCSELs) onto native substrate to fabricate high-quality devices, and afterward, the devices are transferred onto SiN platforms creating a vertical-cavity silicon-integrated laser (VCSIL). In detail, the device transfer can be carried out thanks to a sacrificial layer that is selectively etched after the laser growth onto native substrate, thus enabling the possibility to detach the device for transferring it into the SiN platform. Although the common causes of failure of VCSELs have already been explored [8][9][10], the degradation of novel VCSILs has not been addressed so far. In particular, no one determined whether the micro-transferring technique could be responsible for new failure modes related to VCSILs. In this paper, we analyze the degradation of VCSILs designed for emitting at 845 nm for PICs. We tested the devices via constant current stresses (3.5, 4.0, 4.5 mA) at constant ambient temperature (25°C) to observe the relation between the stress current and the degradation. Our study demonstrated that the degradation is characterized by a diffusion of impurities from the p-side to the active region of the device. Depending on the region crossed by these impurities, the device exhibited different degradation modes. At first, when the impurities are located in the top DBR we measure the degradation of the threshold current, whereas when impurities reach the active region we observe the degradation of both threshold current and sub-threshold emission.

2. SAMPLES UNDER INVESTIGATION

The devices analyzed within this work are vertical-cavity silicon-integrated lasers emitting at 845 nm (Figure 1). The structure, starting from the top, includes a Ti/Pt/Au disk-shaped p-contact that serves both as electrode and as a top reflector. The top DBR (Distributed Bragg Reflector) is p-doped with carbon and consists of 29 mirror pairs of $Al_{0.12}Ga_{0.88}As/Al_{0.90}Ga_{0.10}As$. At the bottom of the p-DBR, within the layer closest to the separate confinement heterostructure (SCH) region, a 30 nm $Al_{0.98}Ga_{0.02}As$-layer is included for the formation, through selective wet oxidation, of an oxide aperture about 4 µm wide. The active area of the laser is located below the aperture and consists of a $1-\lambda$ thick SCH and a multi-quantum-well (MQW) structure containing five 4 nm thick $In_{0.10}Ga_{0.90}As/Al_{0.37}Ga_{0.63}As$ QWs. The bottom DBR is n-doped and is composed of 23 mirror pairs of $Al_{0.12}Ga_{0.88}As/Al_{0.90}Ga_{0.10}As$. A Ni/Ge/Au n-contact is positioned a few DBR mirror pair layers below the active area. At the bottom of the n-DBR, a 527 nm $Al_{0.12}Ga_{0.88}As$ buffer layer is purposedly included to tune the cavity length between the bottom DBR and the diffraction grating. Underneath this layer, a 4 nm GaAs layer serves as an etch stop layer with respect to an $In_{0.49}Ga_{0.51}P$ sacrificial layer, which is required for the micro-transfer-printing process. Below the VCSEL, aligned with the oxide aperture, a diffraction grating was placed to couple the optical mode into a SiN/SiO2 waveguide. Further information regarding the device epitaxy, growth and fabrication can be found in [11].

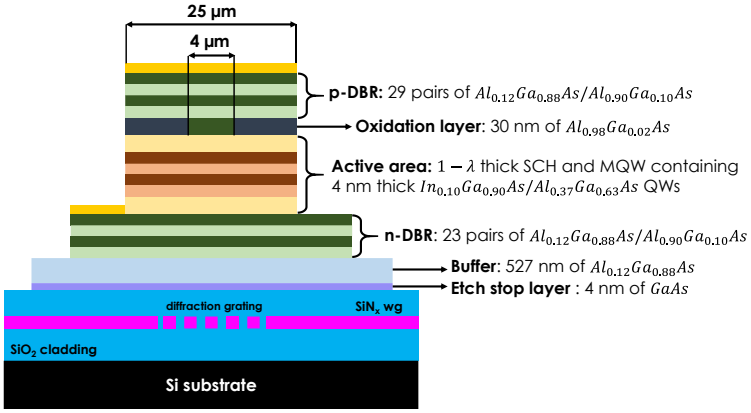

Figure 1. Simplified view: cross section of the samples under investigation.

3. METHODOLOGY

For our experimental purposes, the samples have been aged and characterized on-wafer. Temperature control was achieved through a TEC-controlled baseplate. The electrical characterization was performed by means of an HP 4142 source-meter. The L-I measurements were carried out through a Thorlabs S120VC amplified Si photodiode. The impedance measurements were performed by means of a Keysight E4980A LCR meter. Both stressing and characterization were carried out at a fixed baseplate temperature of T_{AMB}= 25 °C.

To evaluate the degradation kinetics as a function of time, the devices were submitted to a constant-current stress experiment. The stress experiment was interrupted at different stages to evaluate the effects of device degradation by carrying out both electrical (I-V, C-V, and C-f) and optical (L-I) measurements. In this work, we analyze the results of three constant current aging tests carried out at stress levels ranging from 3.5 mA to 4.5 mA. The corresponding stress current density lies within the 27.7 - 35.8 kA/cm^2 window, thus representing a highly accelerated stress condition.

4. OPTICAL DEGRADATION

To analyze the optical characteristics during the stress, we took a representative set of L-I curves taken from the constant current stress at 3.5 mA. In Figure 2, it is shown that above threshold the characteristics exhibit a sinusoidal ripple. This feature is due to the external optical feedback provided by the SiN waveguide and the grating coupler. In terms of degradation, we observe that the threshold current (I_{th}) begins to worsen from the very first seconds of the experiment, but the sub-threshold emission (OP_{sub}) starts to degrade only after a certain amount of time. Given these observations, we decided to divide the experiment into two degradation conditions: condition (A) in which solely the I_{th} is worsening, and condition (B) in which both I_{th} and OP_{sub} are degrading.

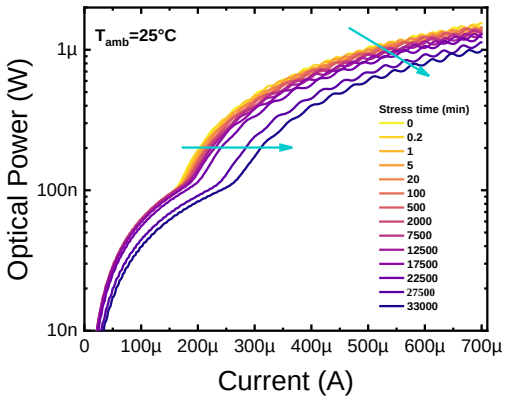

Figure 2. Representative case of L-I degradation (constant current stress at 3.5 mA).

To better distinguish between the two degradation conditions, we repeated the constant current stress for three current levels: 3.5, 4.0, and 4.5 mA. Figure 3 shows the trends of both I_{th} and OP_{sub} to identify the two degradation conditions. Regarding condition (A) we observe that there is no relation with the stress current and the degradation ends when reaching a relative I_{th} variation of 8-15 % with respect to the initial characterization. On the contrary, condition (B) activation occurs earlier when increasing the stress current, so the degradation is accelerated as stress current is increased.

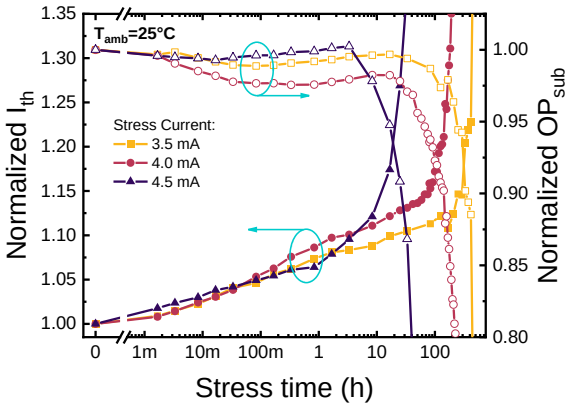

Figure 3. I_{th} and OP_{sub} kinetics: during condition (A) only I_{th} is worsening, condition (B) is reached when both quantities worsen at the same time.

Since I_{th} and OP_{sub} determine the degradation condition ongoing, we tried to correlate these two quantities to discover the degradation root of these devices. Figure 4 shows the I_{th} versus OP_{sub} kinetics. Clearly, during condition (A) the two parameters are not correlated, whereas over condition (B) the two kinetics are linearly correlated. This last feature can be typically ascribed to defects acting as non-radiative recombination centers (NNRCs) in the active region [12]. The presence of defects in the active layers can promote the increment of the current needed to reach the threshold (I_{th} degradation) and worsen the LED-like emission when the device operates below threshold (OP_{sub} degradation).

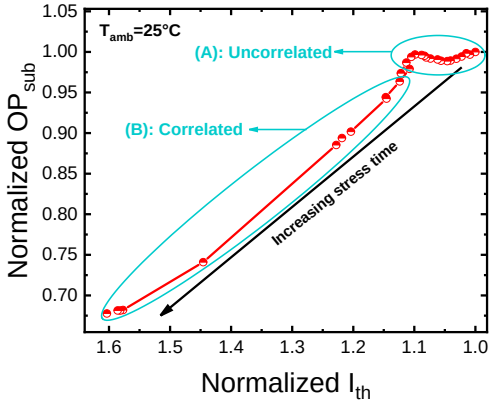

Figure 4. I_{th} vs. OP_{sub}: the linear correlation during degradation condition (B) can indicate the migration of defect in the active layers.

By evaluating the below-threshold rate equation for the threshold carrier density (N_{th}), and assuming that the injection efficiency, η_{inj}, below and above threshold is the same, we can write that [13]:

$$\frac{\eta_i I_{th}}{qV} = \left(A + BN_{th} + CN_{th}^2\right)N_{th} = \frac{N_{th}}{\tau} \quad (1)$$

that yields:

$$I_{th} = \frac{qVN_{th}}{\eta_i \tau} = \frac{qV(A + BN_{th} + CN_{th}^2)N_{th}}{\eta_i} \quad (2)$$

The coefficients A, B, and C are respectively the Shockley-Read-Hall, the radiative and the Auger-Meitner recombination coefficients, q is the electron charge, τ is the average carrier lifetime and V is the volume of the active region. Therefore, the sub-threshold emission, given by [14]:

$$OP_{sub} \propto \frac{N}{\tau} = N(A + BN + CN^2) \tag{3}$$

and the threshold current (Eq. 2), strongly depends on the balance between radiative (BN^2) and non-radiative ($AN + CN^3$) recombination terms. If we assume that the variation of the Auger-Meitner coefficient (CN^3) due to the variation of N_{th} is lower than the increment of the SRH term due to the A coefficient, the strong correlation observed between the trend of I_{th} and OP_{sub} suggests that their worsening during constant-current aging can be ascribed to the increase in SRH recombination rate, possibly due to the generation/relocation of impurities, that reaches the active region in correspondence to the onset of condition (B).

To study in more detail the temporal dependence of degradation we expressed the I_{th} kinetics as a function of the square root of the stress time. According to the results shown in Figure 5, during condition (B) the I_{th} degradation has a square root dependence. This may indicate that a diffusion process is moving impurities or defects toward the active region during this phase. Indeed, when impurities diffuse from a region where their concentration N_0 is constant, the temporal variation in concentration N(x, t) at a given depth x follows Fick's laws of diffusion and can be written as:

$$N(t, x) = \frac{N_0}{\sqrt{4\pi Dt}} e^{-\frac{x^2}{4Dt}} \tag{4}$$

where D is the diffusion coefficient of the moving impurity. Since the amount of defects directly impacts on the non-radiative lifetime (τ_{nr}), the diffusion of impurities can be correlated with the simultaneous degradation of I_{th} and OP_{sub} thus observed during condition (B). Remarkably we can observe that in Figure 5 the change of slope of the linear trend when passing from condition (A) to condition (B). Generally, the change of slope can indicate the variation of the diffusion species or the change in diffusing environment. We are more prone to consider that latter case since it points out that the impurities start moving through a certain region and finally when reaching condition (B), they start to diffuse in the active layers.

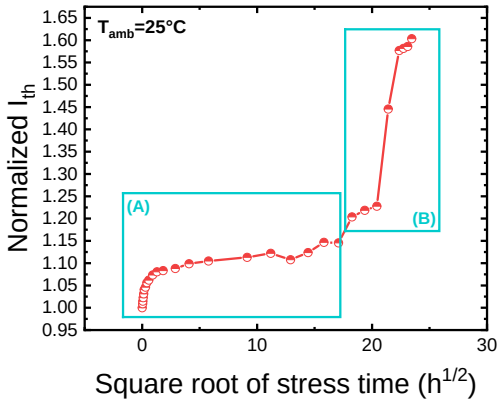

Figure 5. Square root dependence of I_{th} kinetics (constant current stress at 3.5 mA).

This last hypothesis is also useful to determine the root cause of condition (A). This phase does not present the correlation of I_{th} and OP_{sub}, because only the threshold is worsening. Indeed, if during condition (A) the degradation had been localized in the active region also the spontaneous mission (OP_{sub}) would have been affected. Therefore, we suppose that during condition (A) the degradation is causing the worsening of the DBR performances (reflectivity and/or absorption) as:

$$\alpha_{tot} = \alpha_i + \frac{1}{2L} ln\left(\frac{1}{R_1 R_2}\right) \quad (5)$$

where α_{tot} is the total absorption coefficient, α_i represents the internal losses, L is the cavity length and $R_{1,2}$ is the mirror reflectivity. Since the threshold current strongly depends on the optical feedback provided by the DBRs as opposed to the spontaneous emission uncoupled with modes of the cavity, we propose that the degradation taking place over condition (A) is due to the degeneration or diffusion of impurities that are worsening the optical losses of the cavity.

5. ELECTRICAL DEGRADATION

One additional proof of the diffusion-related degradation can be extrapolated from the electrical characteristics. In Figure 6 we compared the optical degradation (OP_{sub}) with the differential resistance behavior (dV/dI). The result of the comparison shows that during condition (A) there is a rapid increase of differential resistance in the device that we ascribed to the relocation of impurities that can passivate the carbon doping (which is the p-type dopant of our devices) which can be responsible for also creating complexes that can induce an increase of series resistance of the DBR characterized by local accumulation of fixed charge. One possible species that could originate such degradation is Hydrogen. Hydrogen was proven to interact with carbon (used as p-type dopant in GaAs) forming H-C_{As} and H-C_{Ga} complexes. This interaction can lead to the passivation of the doping properties of carbon in different III-V materials [15]. This hypothesis also supports the possible generation of defects in the DBR, that can increase the optical absorption. After the first series resistance variation the device exhibits a second increment when reaching condition (B). During condition (B) the optical characterization confirms that the degradation may be located in the active region, therefore when impurities reach the active layers they can originate a second series resistance increment due to the interaction with the narrow and thin semiconductor layers associated with the oxide-confined aperture.

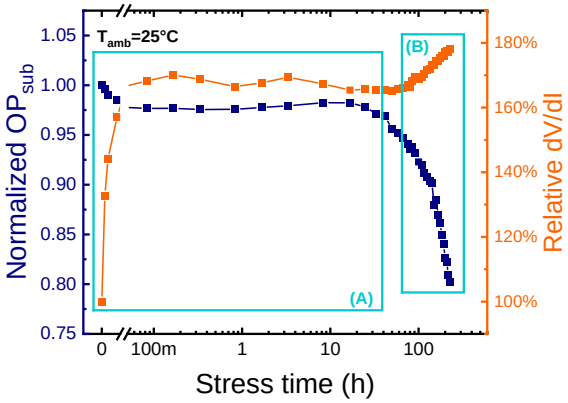

Figure 6. Comparison between differential resistance and optical degradation kinetics.

To better address the regions crossed by the impurities and their effect on the degradation of the devices under test we studied the variation of the small signal impedance induced by the constant current stress experiment. In Figure 7 are reported the variation of the capacitance-voltage (C-V) and capacitance-frequency (C-f) characteristics. From the variation of the C-V curves (Figure 7a) we can observe an increment of the capacitance only above 0.5 V. To investigate the origin of this variation we carried out C-f measurements between 0 and 1 V to study the change in the C-V curves. Figure 7b depicts the C-f characteristics measured at 1 V: the results indicate a capacitance decrease at around 100 kHz which can no longer be probed after the stress.

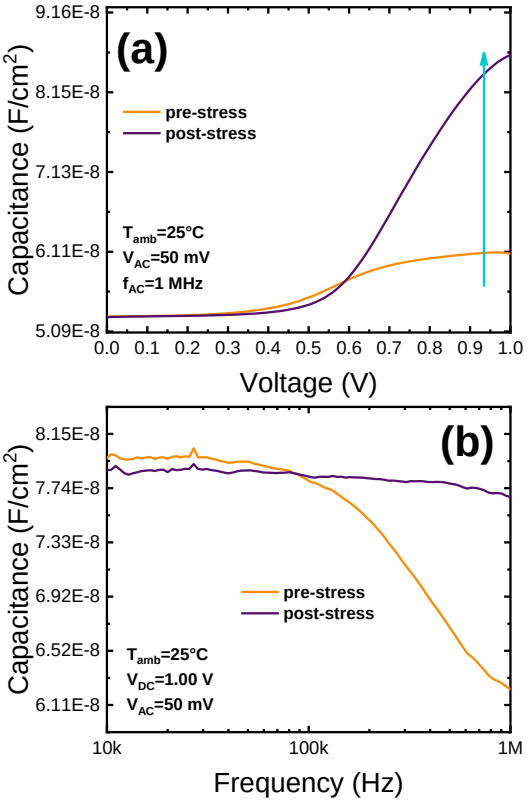

Figure 7. (a) variation of the C-V characteristics. (b) Variation of the C-f characteristics.

The behavior observed in the unaged device can be related to the response of a defect placed at the edge of the space charge region (SCR) being filled and depleted in accordance with the small signal variation (V_{AC}) [16]. By employing thermal admittance spectroscopy (TAS) [17] we related the small signal capacitance inflection point with the thermal emission of the trap, described in the following relation:

$$e(T) = \frac{\omega_i}{0.825} \tag{6}$$

where e(T) is the thermal emission rate at a given temperature T and ω_i is the angular frequency at the inflection point. Analyzing the derivative of capacitance with respect to frequency versus frequency (dC⁄df vs f) over a reasonable temperature range (Figure 8), we measured the small signal capacitance inflection point at different temperatures and by building the related Arrhenius plot, from the mathematical relation expressed by Eq. 7, we found the trap activation energy.

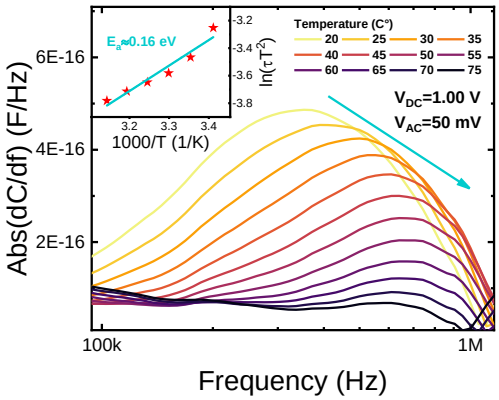

Figure 8. Variation of the derivative of small signal capacitance versus frequency as a function of temperature. The inset shows the results of the Arrhenius plot ($E_a \approx 0.16$ eV).

In the inset of Figure 8 is shown the Arrhenius plot, the resulting E_a is about 0.16 eV indicating the presence of a shallow defect, located close to one of the two band edges.

Based on these experimental observations, we elaborated the following possible explanation for the electrical degradation. The capacitance increment observed in the C-V curves (f_{AC}=1 MHz) in the 0.5÷1 V range is induced by the contact annealing in the early phases of the stress. So, we are assuming that in the unaged device the metal-semiconductor (M-S) junction at the p-side of the device does not perfectly act as an ohmic tunnel junction but exhibits a weak rectifying behavior. Therefore, the electrical model of the AC impedance must consider the main laser diode capacitance (C_{LD}) connected back-to-back with the depletion capacitance added by the M-S junction ($C_{M\text{-}S}$). The total capacitance (C_{tot}) will be:

$$C_{tot} = \frac{C_{LD} \cdot C_{M\text{-}S}}{C_{LD} + C_{M\text{-}S}} \tag{10}$$

In the reverse bias regime, the M-S junction is forward biased, so a very high capacitance is connected in series with the laser capacitance. In this regime, the latter component will be the dominating one as it is the lower of the two. Contrary, in forward bias regime the M-S junction is in reverse bias regime limiting the overall capacitance of the VCSIL. After the contact annealing, the total capacitance is completely determined by the laser capacitance (C_{tot}=C_{LD}) in both bias regimes because the p-contact has become an ohmic tunnel junction. Consequently, the C-f variation can be explained by considering that in the unaged device we can probe the defect as is located in the depletion region of the M-S junction (so located in the upper part of the p-DBR). As a consequence, after the contact annealing, we can no longer detect the defect response, as in this condition is only possible to probe defects located at the edges of the laser SCR. The defect probed in the top DBR in the unaged device may be responsible for the worsening of the DBR performance during the degradation condition (A), which, eventually, reaches the active region and begins the degradation condition (B).

6. CONCLUSIONS

In summary, within this work, we analyzed the degradation modes of 845 nm VCSIL for silicon photonics applications. Based on different constant current experiments at different stress currents (3.5, 4.0, and 4.5 mA), we studied the optical (L-I) and electrical (I-V, C-V, and C-f) characteristics. Based on the experimental results, we recognized two degradation conditions: condition (A) which is the first phase in which only the I_{th} is affected by the stress, and condition (B) in which both I_{th} and OP_{sub} worsen. Our study suggests that the degradation is caused by a diffusion process that starts from the top DBR (condition (A)) and finally reaches the active region (condition (B)). During condition (A) the impurities affect the DBR properties, worsening the absorption and/or the reflection of the mirror, thus affecting solely the I_{th}. The diffusion of impurities is also supported by the increment of series resistance. In addition, also the capacitance measurements confirmed

the presence of a defect close to the p-contact which is no longer detected after the first stages of the stress. We suppose that impurities are passivating the anode in the unaged device forming a Schottky-type contact. After the contact annealing the impurities migrate away, allowing the formation of an ohmic tunnel junction at the p-side. During condition (B) impurities reach the active layers acting as NNRCs worsening both I_{th} and OP_{sub}. The outcome of this analysis suggests that the lifetime of current state-of-the-art VCSILs may be extended by improving the processing/ growth of the p-type contact layers of the devices.

ACKNOWLEDGEMENTS

This research was partly performed within project INTERNET OF THINGS: SVILUPPI METODOLOGICI, TECNOLOGICI E APPLICATIVI, co-founded (2018-2022) by the Italian Ministry of Education, Universities and Research (MIUR) under the aegis of the "Fondo per il finanziamento dei dipartimenti universitari di eccellenza" initiative (Law 232/2016).

REFERENCES

[1] Margalit, N., Xiang, C., Bowers, S. M., Bjorlin, A., Blum, R. and Bowers, J. E., "Perspective on the future of silicon photonics and electronics," Appl. Phys. Lett. 118(22), 220501 (2021).
[2] Chandrasekar, R., Lapin, Z. J., Nichols, A. S., Braun, R. M., Fountain, A. W. and Fountain Iii, A. W., "Photonic integrated circuits for Department of Defense-relevant chemical and biological sensing applications: state-of-the-art and future outlooks," https://doi.org/10.1117/1.OE.58.2.020901 58(2), 020901 (2019).
[3] Fang, Z. and Zhao, C. Z., "Recent Progress in Silicon Photonics: A Review," ISRN Opt. 2012, 1–27 (2012).
[4] Morales, J. M., Cho, P., Bickford, J. R., Pellegrino, P. M., Leake, G. and Fanto, M. L., "Development of army relevant wearable Photonic Integrated Circuit (PIC) biosensors," https://doi.org/10.1117/12.2587098 11749, 98–106 (2021).
[5] V. P. Kalosha, V. A. Shchukin, N. Ledentsov Jr., and N. N. L., "Electrical Properties of Oxide-Confined Vertical-Cavity Surface-Emitting Lasers," Proc. 2011 IEEE Int. Conf. Robot. Biomimetics, 1343–1348 (2011).
[6] Gerthsen, D., Ponce, F. A., Anderson, G. B. and Chung, H. F., "Lattice Mismatch Effects in Gaas Epitaxy on Si and GaP," MRS Online Proc. Libr. 1988 1221 122(1), 21–26 (2011).
[7] Kaur, P., Boes, A., Ren, G., Nguyen, T. G., Roelkens, G. and Mitchell, A., "Hybrid and heterogeneous photonic integration," APL Photonics 6(6) (2021).
[8] Mathes, D., Guenter, J., Hawkins, B., Hawthorne, B. and Johnson, C., "An atlas of ESD failure signatures in vertical cavity surface emitting lasers," Conf. Proc. from Int. Symp. Test. Fail. Anal. 2005, 336–343 (2005).
[9] Xie, S., Herrick, R. W., Chamberlin, D., Rosner, S. J., McHugo, S., Girolami, G., Mayonte, M., Kim, S. and Widjaja, W., "Failure mode analysis of oxide VCSELs in high humidity and high temperature," J. Light. Technol. 21(4), 1013–1019 (2003).
[10] Maeda, K., Sato, M. and Kubo, A., "Quantitative measurements of recombination enhanced dislocation glide in gallium arsenide" J. Appl. Phys. 54, 161 (1983).
[11] Goyvaerts, J., Grabowski, A., Gustavsson, J., Kumari, S., Stassen, A., Baets, R., Larsson, A. and Roelkens, G., "Enabling VCSEL-on-silicon nitride photonic integrated circuits with micro-transfer-printing," Optica 8(12), 1573 (2021).
[12] Buffolo, M., Pietrobon, M., De Santi, C., Samparisi, F., Davenport, M. L., Bowers, J. E., Meneghesso, G., Zanoni, E. and Meneghini, M., "Degradation mechanisms of heterogeneous III-V/Silicon loop-mirror laser diodes for photonic integrated circuits," Microelectron. Reliab. 88–90(May), 855–858 (2018).
[13] Smowton, P. M. and Blood, P., "The differential efficiency of quantum-well lasers," IEEE J. Sel. Top. Quantum Electron. 3(2), 491–498 (1997).
[14] Coldren, L. A., Corzine, S. W. and Mashanovich, M. L., "Wiley: Diode Lasers and Photonic Integrated Circuits, 2nd Edition - Larry A. Scott W. Corzine, Milan L. Mashanovitch," 744 (2012).
[15] Amore Bonapasta, A., "Hydrogen passivation of carbon-doped gallium arsenide," Phys. Rev. B 48(12), 8771–8779 (1993).
[16] Buffolo, M., Caria, A., Piva, F., Roccato, N., Casu, C., De Santi, C., Trivellin, N., Meneghesso, G., Zanoni, E. and Meneghini, M., "Defects and Reliability of GaN-Based LEDs: Review and Perspectives," Phys. status solidi 219(8), 2100727 (2022).
[17] Barbolla, J., Dueñas, S. and Bailón, L., "Admittance spectroscopy in junctions," Solid. State. Electron. 35(3), 285–297 (1992).